

# Study on the Edge Effect in Transport Property Evaluation of Laser-induced Carriers in TlBr Semiconductors

Yusuke Sugai,<sup>1\*</sup> Kenichi Watanabe,<sup>1</sup> Sota Hasegawa,<sup>1</sup>  
Seishiro Tanaka,<sup>1</sup> Mitsuhiro Nogami,<sup>2</sup> and Keitaro Hitomi<sup>2</sup>

<sup>1</sup>Department of Applied Quantum Physics and Nuclear Engineering, Kyushu University,  
744 Motoooka, Nishi-ku, Fukuoka 819-0395, Japan

<sup>2</sup>Department of Quantum Science and Energy Engineering, Tohoku University, Sendai 980-8579, Japan

(Received December 25, 2024; accepted April 2, 2025)

**Keywords:** TlBr semiconductor detector, time of flight, mobility, mobility–lifetime product

TlBr has high detection efficiency and energy resolution and is also considered a semiconductor detector material that can be operated at room temperature. We have developed and improved a system to evaluate the mobility of charge carriers generated by a pulsed laser using the time-of-flight (TOF) technique. With this system, it is possible to evaluate the two-dimensional distribution of charge transport properties by scanning the laser irradiation positions. In this study, we have considered the shape changes of the signal waveform depending on the laser irradiation positions through comparisons between experimental and simulation results. Since the signal shape change is especially severe near the edge of the electrode, this effect is referred to as the edge effect. For the detector having small electrodes compared with the crystal surface, the electric field near the electrode edges is severely disturbed. Consequently, the mobility of electrons generated near the edge of the electrode might be underestimated. To evaluate mobility more accurately, it is desirable to form electrodes over the entire crystal surface as much as possible to create a uniform electric field between the electrodes.

## 1. Introduction

Thallium bromide (TlBr) is expected to be the next-generation semiconductor gamma ray detector.<sup>(1–9)</sup> TlBr has a wide band gap of 2.68 eV, which allows room-temperature operation. It is also composed of high-atomic-number elements (Tl = 81, Br = 35) and has a high density of 7.56 g/cm<sup>3</sup>, which provides the advantage of high detection efficiency. In addition, the melting point of TlBr crystals is low (about 460 °C), and there is one stable crystal structure.<sup>(10)</sup> Therefore, crystal growth is easy, and the low-cost fabrication of detectors can be expected. Recent improvements in the process of TlBr purification using zone melting methods result in higher mobility–lifetime products ( $\mu\tau$  products) of electrons and holes.<sup>(11)</sup> Therefore, some recent studies have shown a high energy resolution of about 1% for 662 keV gamma rays.<sup>(12)</sup>

---

\*Corresponding author: e-mail: [sugai.yusuke.031@s.kyushu-u.ac.jp](mailto:sugai.yusuke.031@s.kyushu-u.ac.jp)  
<https://doi.org/10.18494/SAM5518>

As the next challenge in the TlBr detector development, we will establish a method of stably fabricating large-volume and high-quality detectors. The uniformity of charge transport properties is important to achieve high performance in large-volume detectors. The mobility of charge carriers in semiconductors is an important indicator and is being actively studied.<sup>(13–15)</sup> We have developed a time-of-flight (TOF) measurement system that can evaluate the two-dimensional distribution of carrier mobility within a crystal.<sup>(16)</sup> Carrier mobility is measured from the TOF of charge carriers generated near the crystal surface by pulsed and focused laser irradiation. We can two-dimensionally evaluate the carrier mobility with this measurement system.

Thus far, it has been confirmed that the shape of the signal waveform differs depending on the laser irradiation position. Nearly rectangular signals are obtained when the laser is irradiated to the center of the electrode surface. On the other hand, the signal waveform shape is significantly distorted when the laser is irradiated near the edge of the electrode. In addition, the estimated TOF tends to be longer. In this study, we will investigate the difference in signal waveform shape depending on the irradiation position by comparing the results of experiments and the induced signal simulator. Additionally, we will study the possible region to accurately evaluate carrier mobility.

## 2. Materials and Methods

### 2.1 Sample preparation

TlBr was purified more than 100 times using the zone purification method. A crystal was then grown using the traveling molten zone method. The grown TlBr crystal was cut into a cube with a size of  $5 \times 5 \times 2.36 \text{ mm}^3$  and polished on both  $5 \times 5 \text{ mm}^2$  surfaces. The gold electrodes for the detector were formed on these surfaces by vacuum evaporation. The electrodes were  $4 \times 4 \text{ mm}^2$  in size and about 80 nm in thickness.

### 2.2 TOF measurement system

Figure 1(a) is a conceptual drawing of the TOF measurement system used. The experimental apparatus was encased in a dark box to shield the detector from ambient light. A negative voltage of  $-300$  to  $-800 \text{ V}$  was applied to the cathode electrode using a high-voltage power supply. The laser source employed was a pulsed laser (NPL41C, Thorlabs) with a wavelength of 405 nm and a maximum pulse width of 128 ns. After passing through a neutral density (ND) filter, the laser light was focused by a lens and irradiated onto the cathode side of the detector, forming a focused spot with a diameter of less than 0.5 mm. The laser power was adjusted to 6.4 nJ using the optical density of the filter. The laser irradiation position was modified by moving the detector using a two-axis stage. Figure 1(b) shows the detector illuminated by the laser. A small portion of the laser light passed through the cathode electrode and was absorbed within  $1 \mu\text{m}$  from the crystal surface. As a result, a huge number of electron–hole pairs were generated immediately below the cathode. The holes generated immediately reached the cathode owing to

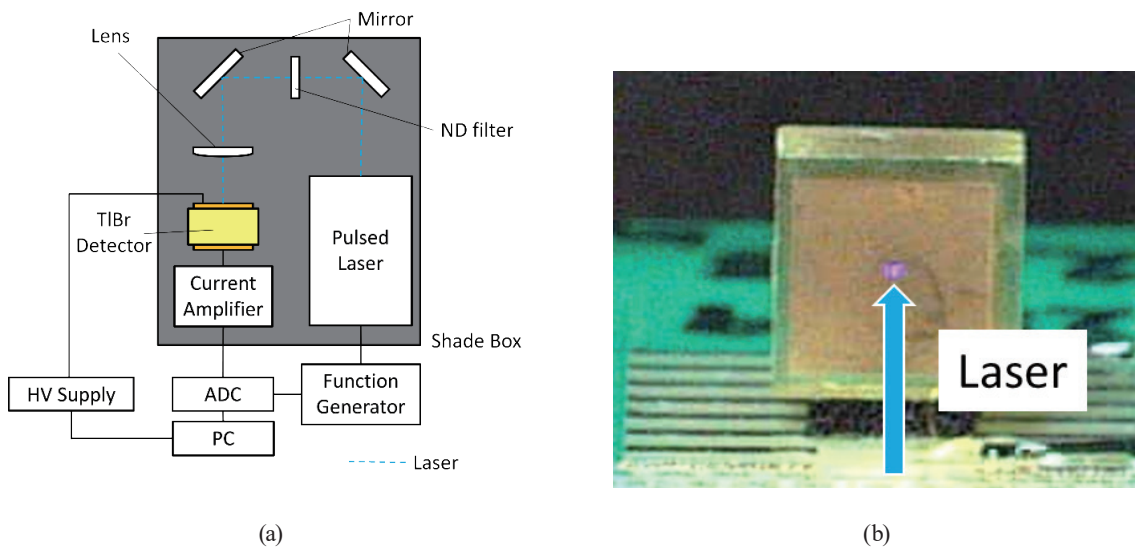


Fig. 1. (Color online) (a) Experimental setup of the TOF measurement system used to characterize the carrier transport properties of the TlBr detector. (b) TlBr detector irradiated with focused laser pulses.

the applied electric field, whereas the electrons moved to the anode side. The induced signal current was amplified by a current amplifier (TIA60, Thorlabs) with a bandwidth from DC to 60 MHz and digitized by an analog-to-digital converter (Model 1820, CLEAR-PULSE). The data were collected and analyzed on a PC. The pulsed laser and ADC were synchronized with 100 Hz trigger pulses.

### 2.3 Simulation of induced signal pulses

To study the difference in waveform shape depending on the laser irradiation position, the induced signal simulator was used. This simulator was developed by our group.<sup>(17)</sup> In this simulator, the weighted potential and the actual electric field were first calculated using the finite element method with Elmer simulation software. After placing the electron–hole pairs at any chosen location, the movement of the carrier was calculated in the simulator. The induced current was calculated on the basis of the Shockley–Ramo theorem according to the movement of the carrier.<sup>(18,19)</sup> In this simulation, the mobility of electrons in the TlBr crystal was assumed to be uniform and  $\mu_e = 25 \text{ cm}^2/\text{Vs}$ . Finally, the simulated signal waveforms were processed using the same signal processing procedure as in the experiments to estimate the carrier TOF.

## 3. Results and Discussion

Figure 2 shows the signal waveforms obtained by irradiating the detector with pulsed laser light at the center and near the edge of the electrode. The simulated signal waveforms are also shown in this figure. In both experiments and simulations, near-rectangular signals were obtained when the laser was irradiated at the center of the electrode surface. In contrast, highly distorted signal waveforms were obtained when the laser was irradiated at the edge of the

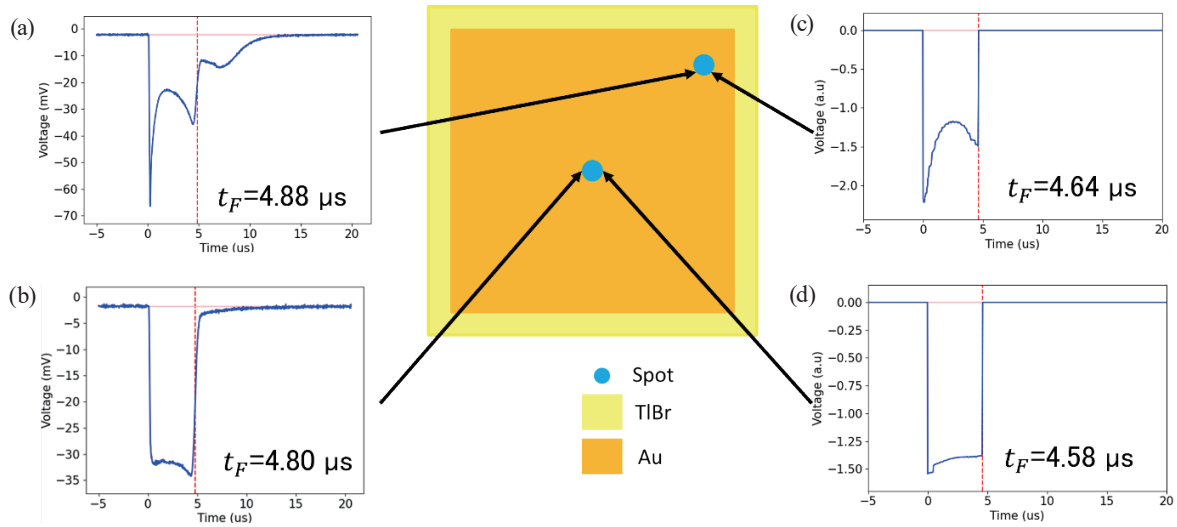


Fig. 2. (Color online) (a) Experimental and (c) simulated signal waveforms obtained by laser irradiation at the edge of the electrode. (b) Experimental and (d) simulated signal waveforms obtained at the center of the electrode.

electrode in both experiments and simulations. The residual component of the signal in Fig. 2(a) (after 5  $\mu\text{s}$ ) is not reproduced in the simulation in Fig. 2(c). This is because this simulation does not consider that the trapped carriers are detrapped and move again. The main component (before 5  $\mu\text{s}$ ) is considered to be the component of carriers that reached the electrode without being trapped. The TOF can be estimated from this component. These signals showed a slightly longer TOF than the waveforms obtained at the center of the electrode. Figure 3 shows the electron trajectory calculated at various laser irradiation positions. The electrons generated just below the center of the electrode move straight toward the anode electrode. On the other hand, the trajectory of electrons generated just below the edge of the electrode is significantly distorted. Figure 4 shows the calculated potentials along each trajectory. The electrons generated just below the center of the electrode pass through constant electric field.

On the other hand, the electrons generated just below the edge of the electrode pass through a stronger electric field near both electrodes. According to the Shockley–Ramo theorem, the induced current  $I(t)$  can be written as

$$I = qvE(\mathbf{r}), \quad (1)$$

where  $q$  is the carrier charge,  $v$  is the velocity, and  $E(\mathbf{r})$  is the weighting field at the carrier position  $\mathbf{r}$ . In this case, the velocity is proportional to the electric field and the weighting field is equal to the electric field. As a result, the induced current is proportional to the square of the electric field. Therefore, because of the distortion of the electric field near the edge of the electrode, the induced current is markedly distorted.

Here, we consider the possible region for the accurate evaluation of the carrier mobility using the induced signal simulator. We simulated the signals induced by the electrons generated at all positions on the electrode and various applied voltages. In this simulation, the mobility is

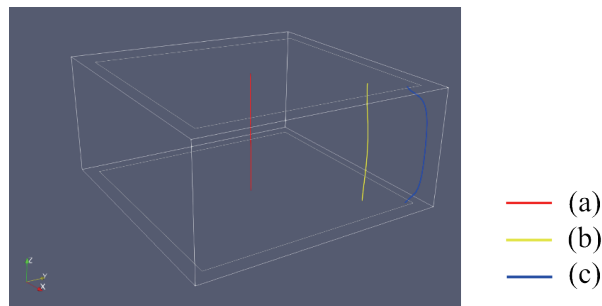


Fig. 3. (Color online) Calculated electron trajectory.

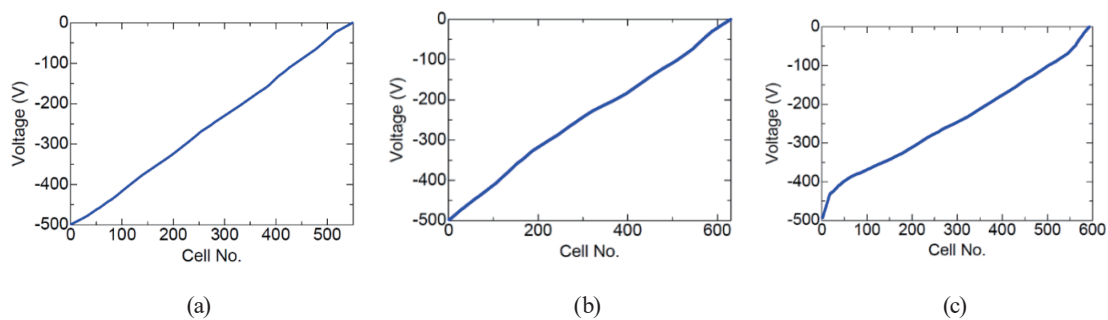


Fig. 4. (Color online) Potentials along electron trajectories. Each graph corresponds to the trajectories shown in Fig. 3.

constant over the entire region. We conducted the same procedure as in the experiments to evaluate the electron mobility. The electron migration velocity can be derived from the thickness of the detector and the pulse width of the induced signal or the TOF. The electron mobility is defined as the proportionality constant between the carrier velocity and the electric field. Therefore, the mobility can be derived from the velocities obtained at various applied voltages. Figure 5 shows the two-dimensional distribution of electron mobility obtained from the simulated signal waveforms. In this simulation, since the mobility is assumed to be constant over the entire region, the evaluated mobility should also be ideally constant. As a result, the electron mobility near the center of the electrode could be accurately evaluated as the expected value. On the other hand, it is difficult to accurately evaluate the mobility near the edge of the electrode. To study the relationship between the electrode sizes and the possible regions for the accurate evaluation of electron mobility, six different detector models with different electrode sizes were modeled and simulated. Figure 6 shows the two-dimensional maps of the evaluated electron mobility in the TlBr detectors with various electrode sizes. The lower limit of the color bars is adjusted to 98% of the expected value ( $=25 \text{ cm}^2/\text{Vs}$ ). The larger the electrode size, the larger the possible region for the accurate measurement of the mobility. Therefore, it is desirable to form electrodes over the entire crystal surface when evaluating the two-dimensional distribution of charge transport properties using this system.

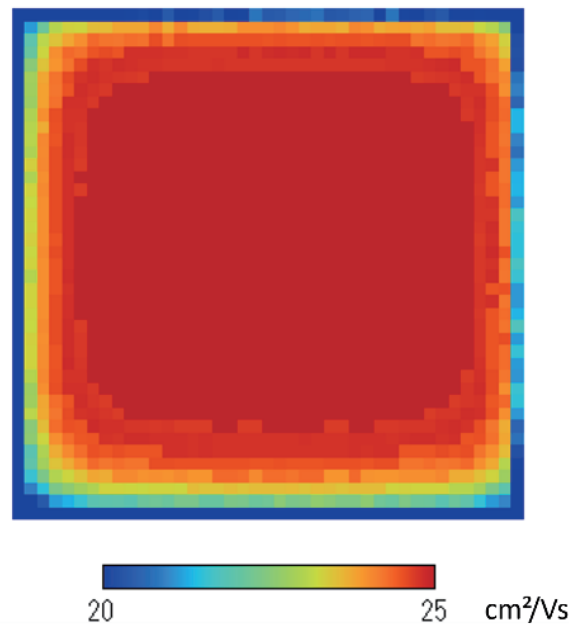


Fig. 5. (Color online) Two-dimensional distribution map of the evaluated electron mobility in the TlBr detector with an electrode size of  $4 \times 4 \text{ mm}^2$ . The crystal size is  $5 \times 5 \text{ mm}^2$ .

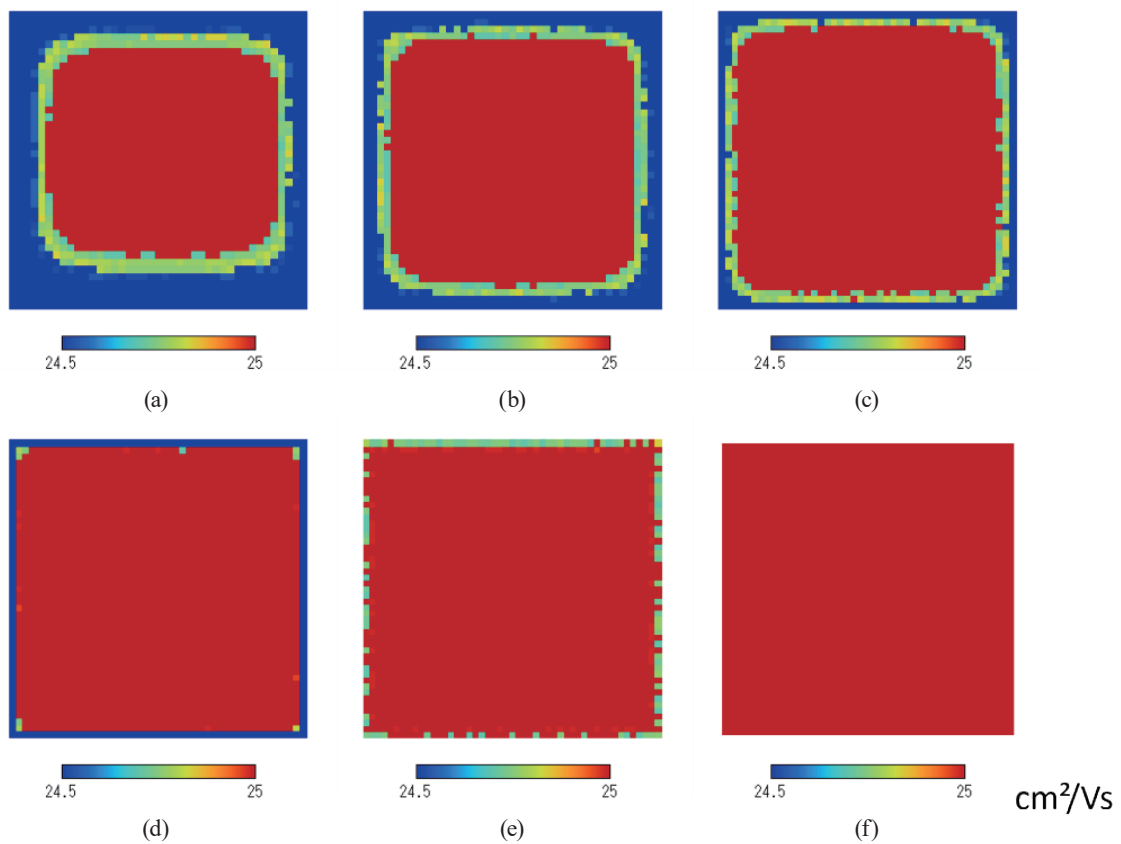


Fig. 6. (Color online) Two-dimensional distribution maps of the evaluated electron mobility in the TlBr detectors. Electrode sizes are (a) 4.0, (b) 4.2, (c) 4.4, (d) 4.6, (e) 4.8, and (f) 5.0  $\text{mm}^2$ , respectively. The lower limit of the color bars is adjusted to 98% of the expected value ( $\approx 25 \text{ cm}^2/\text{Vs}$ ).

## 4. Conclusions

We considered the difference in signal waveform depending on the laser irradiation position by comparing the results of the experiments and the induced signal simulator. Similar waveform trends were observed between the simulation and experimental results, indicating the validity of the induced signal simulator. This simulation makes it possible to objectively advance the design of the optimal detector structure for TOF measurements. If the electrodes are small relative to the crystal, the electric field is not uniformly distributed, and the electrons do not move straight toward the electrode. As a result, the electron mobility near the electrode edge is likely to be underestimated. For this reason, it is important in mobility measurements to form electrodes having the same size as the crystal face to generate a uniform electric field between the electrodes.

## Acknowledgments

This work was partially supported by JSPS KAKENHI Grant Number JP 22H02008. It was also partially supported by the Cooperative Research Project of the Research Institute of Electronics, Shizuoka University.

## References

- 1 K. Hitomi, T. Murayama, T. Shoji, T. Suehiro, and Y. Hiratate: Nucl. Instrum. Methods Phys. Res. A **428** (1999) 372.
- 2 K. Hitomi, O. Muroi, T. Shoji, T. Suehiro, and Y. Hiratate: Nucl. Instrum. Methods Phys. Res. A **436** (1999) 160.
- 3 T. Onodera, K. Hitomi, T. Shoji, and Y. Hiratate: Nucl. Instrum. Methods Phys. Res. A **525** (2004) 199.
- 4 K. Hitomi, T. Onodera, T. Shoji, and Z. He: Nucl. Instrum. Methods Phys. Res. A **578** (2007) 235.
- 5 K. Hitomi, T. Shoji, and Y. Niizeki: Nucl. Instrum. Methods Phys. Res. A **585** (2008) 102.
- 6 K. Hitomi, Y. Kikuchi, T. Shoji, and K. Ishii: Nucl. Instrum. Methods Phys. Res. A **607** (2009) 112.
- 7 B. Donmez, Z. He, H. Kim, L. J. Cirignano, and K. S. Shah: Nucl. Instrum. Methods Phys. Res. A **623** (2010) 1024.
- 8 K. Hitomi, T. Shoji, and K. Ishii: J. Cryst. Growth **379** (2013) 93.
- 9 K. Hitomi, T. Onodera, S-Y. Kim, T. Shoji, and K. Ishii: Nucl. Instrum. Methods Phys. Res. A **747** (2014) 7.
- 10 Carl W. F. T. Pistorius and J. B. Clark: Phys. Rev. **173** (1968) 692.
- 11 K. Hitomi, T. Onodera, and T. Shoji: Nucl. Instrum. Methods Phys. Res. A **579** (2007) 153.
- 12 K. Hitomi, T. Tada, T. Onodera, S-Y. Kim, Y. Xu, T. Shoji, and K. Ishii: IEEE Trans. Nucl. Sci. **60** (2013) 1156.
- 13 K. Suzuki, M. Shorohov, T. Sawada, and S. Seto: IEEE Trans. Nucl. Sci. **62** (2015) 433.
- 14 K. Suzuki, T. Sawada, and K. Imai: IEEE Trans. Nucl. Sci. **58** (2011) 1958.
- 15 M. Funahashi: In Organic Semiconductors for Optoelectronics, H. Naito, Ed. (John Wiley & Sons Ltd, Hoboken, 2021) Chap. 6.
- 16 Y. Sugai, K. Watanabe, S. Hasegawa, K. Hitomi, and M. Nogami: Sens. Mater. **36** (2024) 155.
- 17 S. Hasegawa, K. Watanabe, Y. Sugai, K. Hitomi, and M. Nogami: Sens. Mater. **36** (2024) 163.
- 18 W. Shockley: J. Appl. Phys. **9** (1938) 635.
- 19 S. Ramo: Proc. IRE **27** (1939) 584.

